


Article

Low Temperature Methanation of CO₂ on High Ni Content Ni-Ce-ZrO₈ Catalysts Prepared via One-Pot Hydrothermal Synthesis

Vissanu Meeyoo ^{1,*}, Noppadol Panchan ¹, Nat Phongprueksathat ¹, Atsadang Traitangwong ², Xinpeng Guo ², Chunshan Li ² and Thirasak Rirksomboon ^{3,4}

¹ Centre for Advanced Materials and Environmental Research, Mahanakorn University of Technology, Bangkok 10530 Thailand; npd.panchan@icloud.com (N.P.); nat.pt@outlook.com (N.P.)

² Beijing Key Laboratory of Ionic Liquids Clean Process, State Key Laboratory of Multiphase Complex System, Institute of Process Engineering, Chinese Academy of Sciences, Beijing 100190, China; atsadangt@hotmail.com (A.T.); guoxinpeng123@126.com (X.G.); csl@ipe.ac.cn (C.L.)

³ The Petroleum and Petrochemical College, Chulalongkorn University, Bangkok 10330, Thailand; T.Rirksomboon@unb.ca

⁴ Center of Excellence for Petrochemical and Materials Technology, Chulalongkorn University, Bangkok 10330, Thailand

* Correspondence: vissanu@mut.ac.th

Received: 30 October 2019; Accepted: 23 December 2019; Published: 26 December 2019



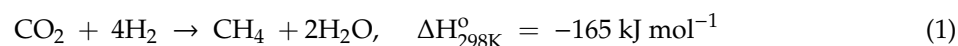
Abstract: Ni-Ce-Zr-O₈ catalysts were prepared via one-pot hydrothermal synthesis. It was found that Ni can be partially incorporated into the Ce-Zr lattice, increasing surface oxygen species. The catalysts possess high surface areas even at high Ni loadings. The catalyst with Ni content of 71.5 wt.% is able to activate CO₂ methanation even at a low temperature (200 °C). Its CO₂ conversion and methane selectivity were reported at 80% and 100%, respectively. The catalyst was stable for 48 h during the course of CO₂ methanation at 300 °C. Catalysts with the addition of medium basic sites were found to have better catalytic activity for CO₂ methanation.

Keywords: CO₂ methanation; nickel catalyst; one-pot hydrothermal synthesis; ceria; zirconia

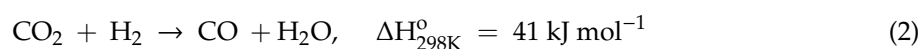
1. Introduction

Catalytic hydrogenation of CO₂ has drawn considerable attention due to its potential for the production of methane or other useful hydrocarbons. For CO₂ methanation, the greenhouse gas (CO₂) is consumed, and converted to methane, promoting energy regeneration, and methane can be used as a clean fuel. This reaction (Rxn. 1) occurs competitively with reverse water gas shift reaction (Rxn. 2) and CO methanation reaction (Rxn. 3) as expressed below.

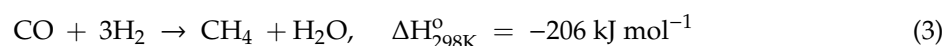
CO₂ methanation (CDM):



Reverse water gas shift (RWGS):



CO methanation (CMM):



It was reported that CO₂ methanation (CDM) could occur through CO intermediates through which CO₂ had initially undergone the reverse water gas shift then was followed by CO methanation (CMM) [1,2]. With weak basic supports such as Ce-Zr oxide supports, CO₂ formed carbonates on the surface followed by being hydrogenated to yield formate, and then CH₄ [3–5]. Due to the exothermic nature of the CDM reaction, CO₂ conversion is not favorable at a high-temperature operation; therefore, it would be desirable to make use of a catalyst which possesses remarkably high catalytic activity at low temperatures in the CDM reaction. Typically, Ni and specific noble metals such as Ru, Rh, and Pd are selected as active species on various supports [6–16]. Although Ni-based catalysts were commonly utilized due to their low cost and high activity [17–20], they were prone to suffer from the deactivation by metal sintering and carbon deposition even at low temperatures [21,22]. The nature of support also affected the state of an active phase involved in the adsorption and catalysis [23]. Apparently, Ce-Zr mixed oxides were demonstrated as good catalyst support potential for methanation because of their advantages, including good redox properties, high thermal stability, as well as resistance to sintering and coke formation [24–26]. Moreover, CeO₂ was found to improve CO₂ adsorption and active metal dispersion resulting in better catalytic activity [3]. Nonetheless, most Ni-based catalysts were not active at low temperatures [18–20]. According to the literature, loading a high amount of Ni could improve the catalytic activity by offering more adsorption arenas for the migration of intermediate species [27–30]; however, high metal loading via the conventional impregnation method often resulted in the low dispersion of the bulk oxide and channel blocking by the formation of bulk metal oxide clusters [31]. Therefore, the method to prepare high nickel content catalysts with good promoting effects of the support is essential.

In this work, the high Ni-loading Ni-Ce-ZrO₈ catalysts were prepared via one-pot hydrothermal synthesis for which such high surface area catalysts with Ni loading of up to 71.5 wt.% were achieved. The results of their catalytic activity for CO₂ methanation investigated in the temperature range of 200–600 °C were herein elucidated.

2. Results and Discussion

2.1. BET Surface Areas, XRD, XPS, H₂-TPR, and CO₂-TPD Analyses

The results showed that Brunauer–Emmett–Teller (BET) surface areas of the catalysts synthesized are in the range of ca. 145–189 m² g^{−1} (Table 1). Noticeably, there is no directly reciprocal correlation between the surface area and Ni loading. Unlike the conventional impregnation method, the one-pot hydrothermal method provided a considerably high surface area of Ni-Ce-ZrO₈ catalysts, especially for the catalysts with such high Ni loadings of 62.5 and 71.5 wt.%, the surface areas of ca. 156 and 158 m² g^{−1} could be, respectively, observed. The pore volume of the catalysts still remained high, indicating that there was no channel blocking due to the formation of bulk metal oxide clusters. It was noticed that the pore diameter increases with increasing Ni content. As determined, the pore diameters range from 4.67 to 15.58 nm (Supplementary Figure S1).

Table 1. Textural and crystal structural properties of Ni-Ce-ZrO₈ catalysts.

Catalyst (Ni/Ce Ratio)	Ni Content (wt.%)	Surface Area (m ² g ^{−1})	Pore Size (nm)	Pore Volume (cm ³ g ^{−1})	Crystallite Size of CeO ₂ (nm)	Lattice Parameter ^a (Å)
Ni0.15	5.9	188.56	4.67	0.11	67.78	5.4182
Ni0.45	15.8	145.20	6.01	0.15	61.06	5.4182
Ni0.75	23.8	164.44	5.91	0.20	54.97	5.4126
Ni4.0	62.5	156.44	15.01	0.63	31.77	5.4182
Ni6.0	71.5	158.45	15.58	0.74	31.12	5.4108

^a Pure CeO₂ lattice parameter = 5.4201 Å.

The X-ray diffraction (XRD) patterns of the catalysts are shown in Figure 1. The results showed a typical cubic fluorite structure of CeO₂ indices at 2θ = 28°, 33°, 48°, and 58° for all the catalysts with varied intensity. At lower Ni contents (below ca. 25 wt.%), the absence of anticipated peaks pertaining to Ni species is observed with a maintained peak intensity of the cubic fluorite structure, indicating

dissolution of Ni in Ce-Zr mixed oxide structure. However, at higher Ni contents, the appearance of additional peaks at 37° , 43° , 63° , and 75° attributed to NiO phases is observed with a decrease in peak intensity of the cubic fluorite structure inferring the existence of free NiO species on the catalyst surface. In addition, it was found that the incorporation of Ni into the Ce-Zr mixed oxide via one-pot hydrothermal synthesis has a slight influence on the lattice parameter of pure cerium oxides. The CeO₂ crystallite size was found to decrease with increasing Ni loading (Table 1). This might be because Ni ionic radius is smaller than the cerium ionic radius [32].

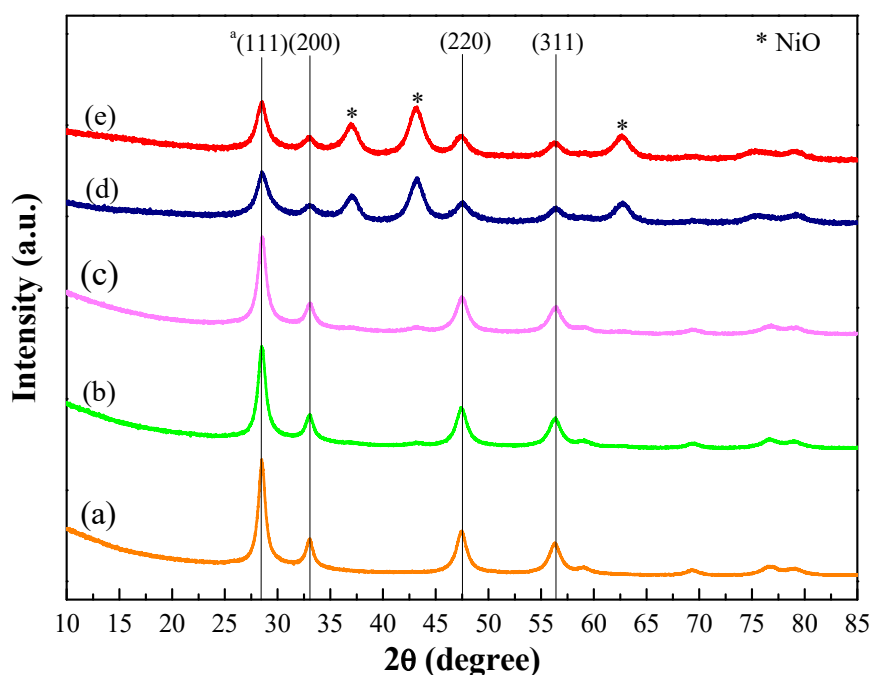


Figure 1. XRD patterns of Ni-Ce-ZrO₂ catalysts; (a) Ni_{0.15}, (b) Ni_{0.45}, (c) Ni_{0.75}, (d) Ni_{4.0}, and (e) Ni_{6.0}; the numerical value after Ni represents the Ni/Ce molar ratio as well as ^a Cubic phase of CeO₂.

Figure 2 shows the reducibility of the catalysts obtained by the temperature-programmed reduction (H₂-TPR) technique. The results showed that at Ni loading below 25 wt.%, there was no obvious reduction peak of NiO. A small broaden peak beginning at ca. 300 °C was observed with catalysts having 15.8 (Ni_{0.45}) and 23.8 (Ni_{0.75}) wt.% Ni. This suggested that at lower Ni loadings, most of Ni could be incorporated into the Ce-Zr lattice [33] until it reached saturation, resulting in the increased oxygen surface reduction. Furthermore, the excess nickel might form free small NiO particles well dispersed on the surface of the Ni-Ce-ZrO_δ, which cannot be detected by XRD. At higher Ni loadings, there is a reduction peak of NiO centered at ca. 490 °C, indicating that the NiO species formed a larger cluster and strongly interacted with Ce/Zr oxides. Noticeably, the peak was more intense as the Ni loading was increased.

Temperature-programmed desorption (CO₂-TPD) technique was used to investigate the basic strength and basicity of the catalysts. Figure 3 shows two major CO₂ desorption peaks located at 100–200 °C and 400 °C indicating weak and moderate Lewis basic sites, respectively [3]. It was found that the amount of CO₂ adsorption is related to the amount of Ni loading by which the moderate basic sites were present in the catalysts containing Ni of more than ca. 25 wt.%. According to the X-ray photoelectron spectroscopy (XPS) data, as shown in Figure 4, it was found that with increasing Ni content, the amount of OH[−] groups and surface oxygen vacancies was found to increase (Figure 4a). The presence of the OH[−] groups was subjected to the desorption of CO₂ at a low temperature [3], while the surface oxygen species responsible for the desorption at medium temperatures were due to the enhancement of the NiO_x lattice oxygen dominating the overall composition. As evidenced, the stronger spectrum of Ni2p_{3/2} (Ni²⁺) (Figure 4b) was observed with the lessen spectra of Zr3d_{3/2} (Figure 4c) and Ce3d (Figure 4d). This suggested that the presence of more pronounced surface nickel

species resulting from a high Ni loading by one-pot hydrothermal synthesis would give rise to a better activity. Moreover, it was found that the Ni6.0 catalyst has larger amounts of both OH⁻ group and surface oxygen vacancy, which help promote CO₂ adsorption. More details related to XPS analysis are presented in Supplementary Table S1.

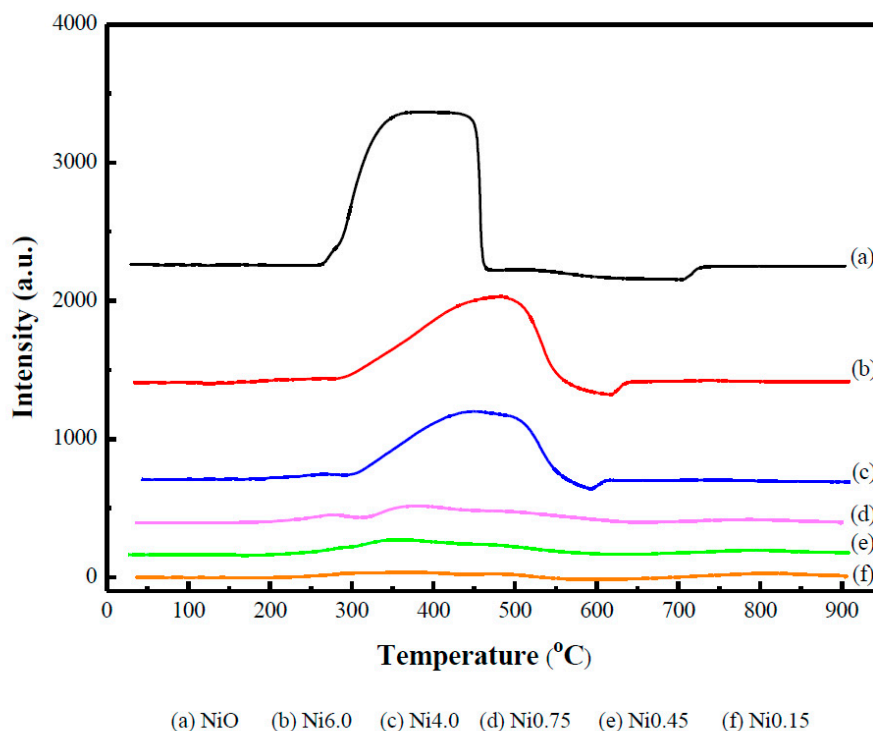


Figure 2. H₂-TPR profiles of Ni-Ce-ZrO₈ catalysts.

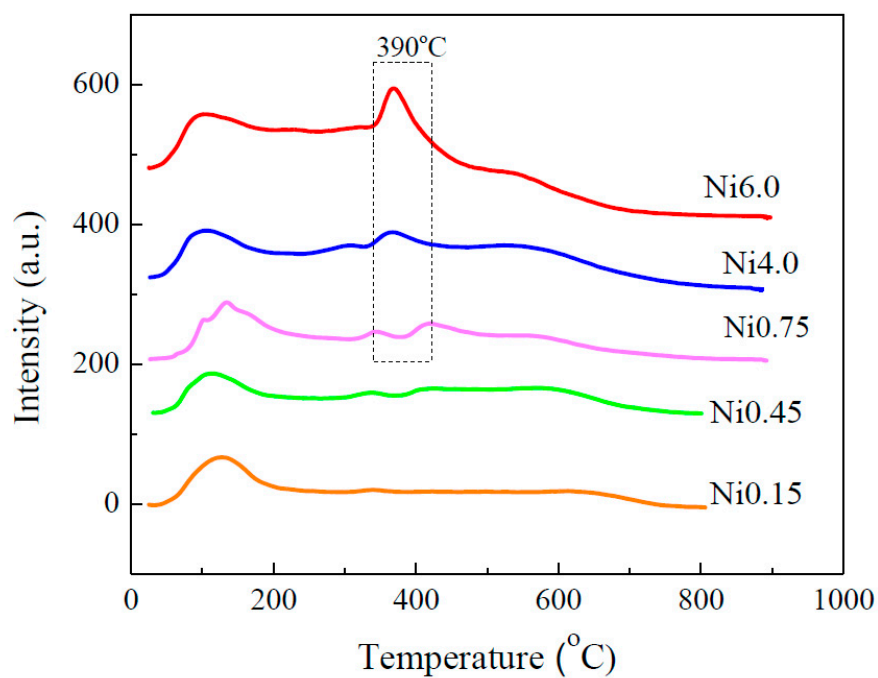


Figure 3. CO₂-TPD profiles of Ni-Ce-ZrO₈ catalysts.

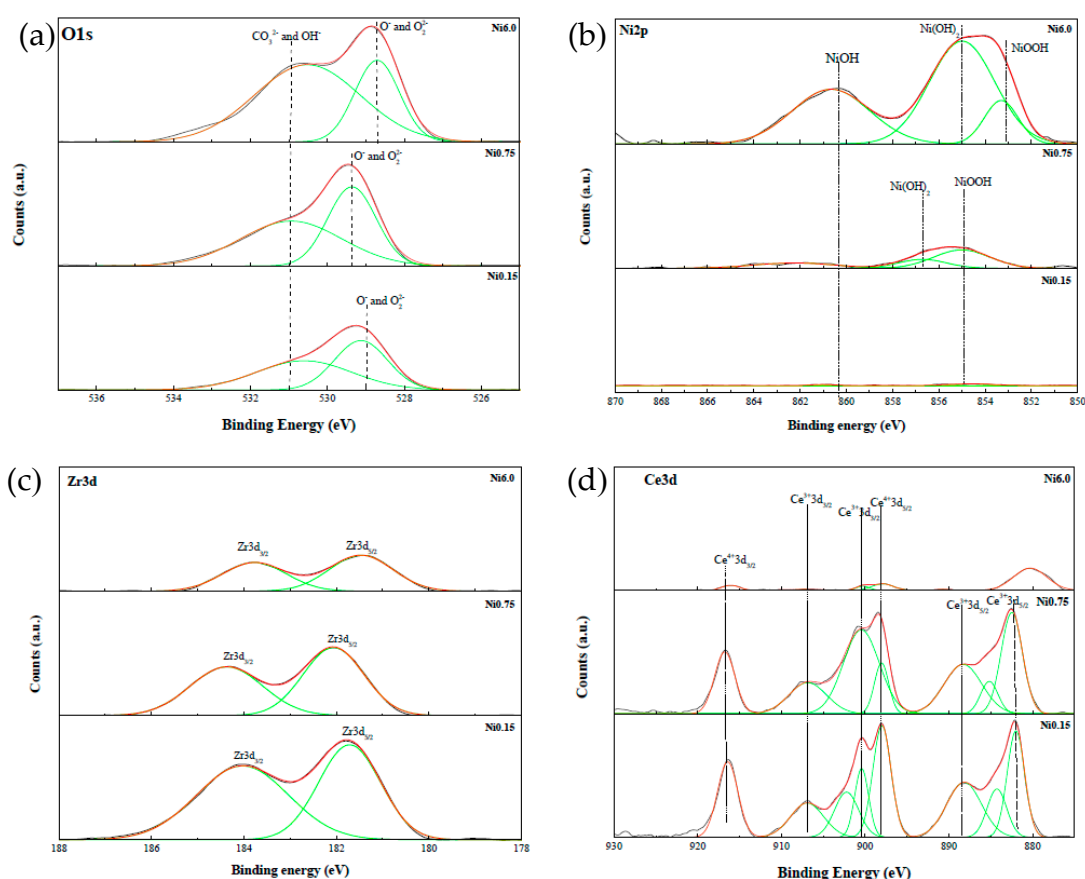


Figure 4. XPS spectra of Ni-Ce-ZrO₈ catalysts; (a) O1s, (b) Ni2p, (c) Zr3d, and (d) Ce3d.

2.2. CO₂ Methanation

Figure 5 illustrates the CO₂ conversion and methane selectivity for Ni-Ce-ZrO₈ catalysts in the CO₂ methanation. Of most catalysts, CO₂ conversion is increased with increasing reaction temperature until its maximum conversion is reached, then, followed by the slight decline approaching the equilibrium conversion due to the thermodynamic limitations of this reaction. However, the maximum CO₂ conversion cannot be observed with the lowest Ni loading catalyst (Ni0.15). A similar trend for CH₄ selectivity can be obtained for all the catalysts as they deviated from the maximum value in an adverse exponential manner when the temperature was raised over 300 °C. Noteworthy, each of the catalysts yields different minimum CH₄ selectivity at the same reaction temperature of 600 °C. At a given temperature, Ni-Ce-ZrO₈ catalysts with high Ni content demonstrate better performance for CO₂ methanation by which the catalytic activity is increased in the order of Ni loading: Ni0.15 < Ni0.45 < Ni0.75 < Ni4.0 < Ni6.0. Interestingly, the catalyst with 71.5 wt.% Ni loading (Ni6.0) gave the highest activity even at a low temperature (200 °C) with a turnover frequency (TOF) of 0.66 h⁻¹ (Table 2), whereas the other catalysts yielded a minute activity at such a temperature. This is because the Ni6.0 catalyst possesses the highest amounts of OH⁻ group and surface oxygen species, as evidenced by CO₂-TPD and XPS results (Figures 3 and 4). Since OH⁻ group and oxygen species adsorbed CO₂ to form bidentate formate and monodentate formate intermediates, respectively [3], the formation of these intermediate species could effectively induce the catalytic hydrogenation of CO₂ molecules by consuming active H species existing on the Ni-Ce-Zr surfaces to form a C-H bond [32], thus, significantly enhancing the CO₂ conversion. Moreover, increasing Ni content also provides more adsorption arenas for the migration of intermediate species, and hence, leading to a high activity [34]. Similar findings on the other supports were reported elsewhere [28–30,35]. According to the obtained results and analyses, it can be postulated that a decrease in the methanation activity of the catalyst

would be related to the consumption of active H species. For low Ni content catalysts, this is attributed to low reaction temperature, which is not conducive to the activation of reactant H₂ molecules to form active H species for the CO₂ methanation reaction. Moreover, the formation of monodentate formate was nearly unattainable for these catalysts due to the lack of medium basic sites. However, these catalysts achieve high CH₄ selectivity. The CH₄ selectivity was attained with ca. 100% for all the catalysts at a low temperature of 200 °C. However, it was found to decrease drastically at the temperature above 500 °C because of a reverse water-gas shift reaction. It should be pointed out that at the temperature above 300 °C, low Ni content catalysts seem to promote a reverse water-gas shift reaction. Nevertheless, this could be explained that at low Ni concentrations, Ni can be incorporated into Ce-Zr lattice generating more oxygen vacancies on the surface. Since the amounts of active H species are less with low Ni content on the surface, some intermediates are desorbed as CO without the formation of C-H bonds [32]. In addition, the Ni6.0 catalyst showed no sign of deactivation during CO₂ methanation at 300 °C for 48 h (Supplementary Figure S2). The amount of carbon deposition on the spent catalyst was detected by TG analysis at less than 1 wt.% (not shown), and there was also no clear evidence of carbon deposition observed by transmission electron microscope (TEM) (Supplementary Figure S3).

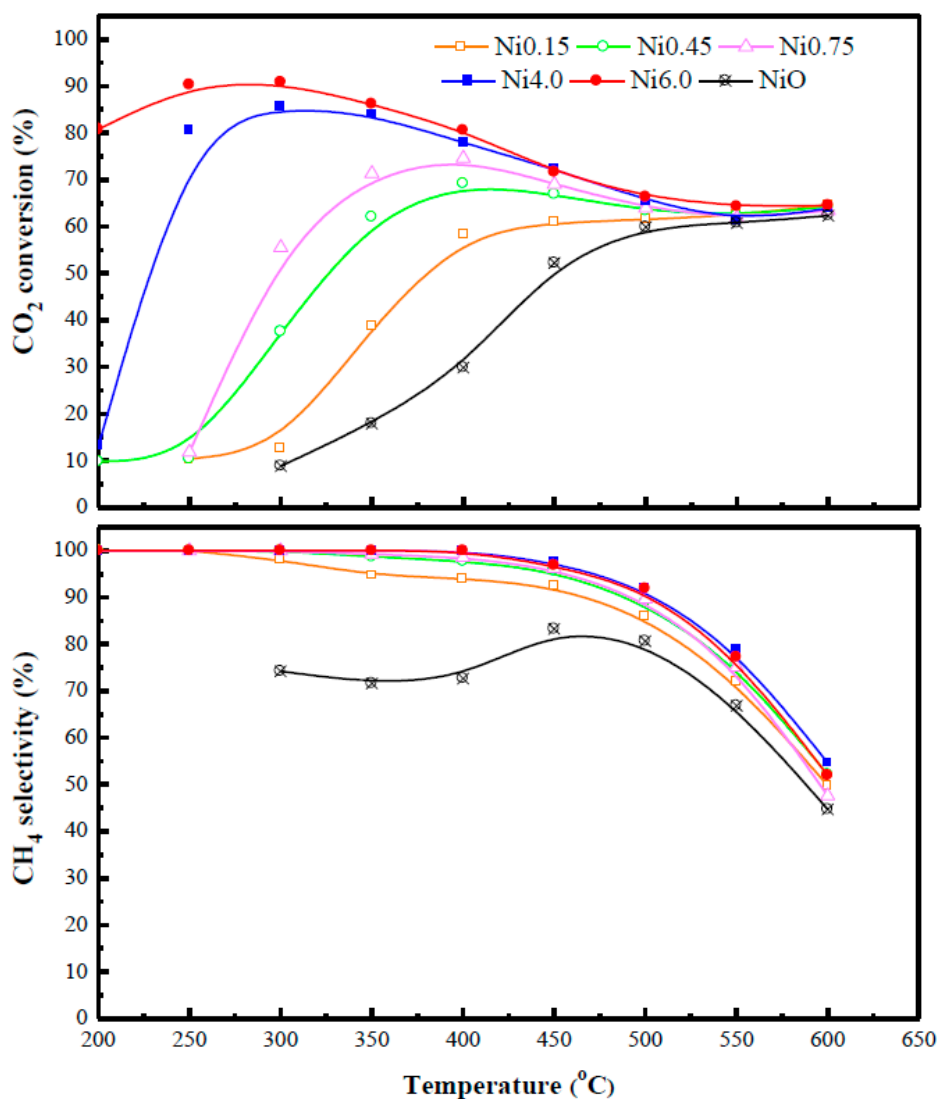


Figure 5. CO₂ conversion and CH₄ selectivity of Ni-Ce-ZrO₈ catalysts for the methanation of CO₂.

Table 2. Summary of the reaction results of CO₂ methanation.

Catalyst	200 °C		300 °C		Ref.
	X _{CO2} (%)	TOF (h ⁻¹)	X _{CO2} (%)	TOF (h ⁻¹)	
Ni0.15	-	-	12.54	1.25	This work
Ni0.45	9.83	0.36	37.57	1.39	
Ni0.75	-	-	55.56	1.36	
Ni4.0	13.13	0.12	85.62	0.81	
Ni6.0	80.79	0.66	90.86	0.74	
30Ni-Ce _{0.9} Zr _{0.1} O ₂	10.30	0.31	-	-	[36]
40Ni-Ce _{0.9} Zr _{0.1} O ₂	7.80	0.22	-	-	
50Ni-Ce _{0.9} Zr _{0.1} O ₂	10.10	0.26	-	-	
NiO/Ce _{0.25} Zr _{0.75} O ₂	-	-	16	0.39	[37]
NiO/Ce _{0.50} Zr _{0.50} O ₂	-	-	21	0.52	
NiO/Ce _{0.75} Zr _{0.25} O ₂	-	-	21	0.52	
Ni/CZ	3.7	0.01	-	-	[38]
Ni(4.4)@CZ	9.5	0.01	-	-	

3. Experimental Section

3.1. Catalyst Preparation

Ni-Ce-ZrO₈ catalysts were prepared via one-pot hydrothermal synthesis adopted from what reported elsewhere [32]. The molar ratio of Ce/Zr was maintained at 3:1 with the alteration of the Ni/Ce molar ratio. Typically, 0.1 M of metal salt solutions were premixed to the desired ratio of Ni/Ce/Zr. The resultant solution was then mixed with a 0.4 M of urea solution at the metal-to-urea ratio of 2:1. Then, the solution was transferred to a Teflon lining autoclave and kept at 105 °C for 50 h. The precipitate was washed with ethanol and dried at 105 °C prior to calcination at 500 °C for 4 h.

3.2. Catalyst Characterization

The catalysts were characterized for Brunauer–Emmett–Teller (BET) surface areas using a Micromeritics ASAP 2460 apparatus (Norcross, GA, U.S.A.). To ensure the accuracy of the data, the samples were outgassed at 350 °C for 6 h before being subjected to N₂ adsorption. X-Ray diffraction (XRD) patterns were attained and analyzed using a Rigaku Smart Lab X-ray powder diffractometer (Rigaku Corporation, Tokyo, Japan) with Cu K α radiation. The XRD patterns were recorded with 2 θ ranged from 10° to 90°. Temperature-programmed reduction (H₂-TPR) and temperature-programmed desorption (CO₂-TPD) were carried out using in-house equipment. The catalyst was pretreated under a flow of N₂ at 400 °C for 30 min prior to running the TPR and TPD experiments and then cooled down to room temperature. For H₂-TPR, a 5% H₂/N₂ gas was used as a reducing gas. The sample temperature was raised at a constant rate of 10 °C min⁻¹ from room temperature to 950 °C. For CO₂-TPD, CO₂ as a reactant gas was introduced with a flow rate of 30 mL min⁻¹ into a sample cell at room temperature for 1 h, then Ar with a flow rate of 30 mL min⁻¹ was introduced for the desorption experiment using the same heating rate from room temperature to 800 °C. The amounts of H₂ consumption and CO₂ desorbed were determined from a TCD signal validated by appropriate calibrations. X-ray photoelectron spectroscopy (XPS) measurements were carried out on an Axis Supra (Kratos Analytical Ltd., Wharfedale, Manchester, U.K.) using a monochromatic AlK α source. The surface charging effects were corrected with the C1's binding energy value of 284.6 eV.

3.3. CO₂ Methanation

CO₂ methanation was carried out in a continuous flow packed bed reactor (inner diameter (i.d.) 0.6 mm) placed in a tubular furnace equipped with temperature controllers. Typically, 0.05 g of catalyst was packed between layers of quartz wool. Prior to the reaction, the catalyst was reduced in situ using H₂ with a flow rate of 50 mL min⁻¹ at 500 °C for 2 h, and then the temperature was cooled to

150 °C in Ar. The CO₂ methanation was carried out in the temperature range of 200–600 °C with a GHSV (gas hourly space velocity) of 10,000 h⁻¹. The H₂/CO₂ molar ratio was 4:1 with a total flow rate of 50 mL min⁻¹. The water in the product stream was condensed, and the permanent gases were analyzed using a Shimadzu GC14B gas chromatograph (Shimadzu Corp., Kyoto, Japan) equipped with a TCD (thermal conductivity detector) and installed with Alltech CTR I and Supelco Carboxen columns. The CO₂ conversion and methane selectivity were calculated by the following equations.

$$\text{CO}_2 \text{ conversion (\%)} = \frac{[\text{CO}_2]_{\text{in}} - [\text{CO}_2]_{\text{out}}}{[\text{CO}_2]_{\text{in}}} \times 100 \quad (4)$$

$$\text{CH}_4 \text{ selectivity (\%)} = \frac{\text{CH}_4}{[\text{CO}_2]_{\text{in}} - [\text{CO}_2]_{\text{out}}} \times 100 \quad (5)$$

4. Conclusions

In conclusion, Ni-Ce-ZrO₈ catalysts were successfully prepared via one-pot hydrothermal synthesis with the maximum Ni loading of up to 71.5 wt.%. The obtained catalysts possess high surface areas even at high loading Ni contents and provide good catalytic activities and CH₄ selectivity for CO₂ methanation. It was found that Ni6.0 was the most active catalyst achieving the low-temperature CO₂ conversion of ca. 80% at 200 °C and 100% CH₄ selectivity. This is believed to owe to the two main basic sites, which facilitate the formation of the intermediates and the ability to activate the active H species at a low temperature. The presence of OH⁻ groups enhances the catalytic activity at low temperatures while that of surface oxygen vacancies promotes the catalytic activity at moderate temperatures.

Supplementary Materials: The following are available online at <http://www.mdpi.com/2073-4344/10/1/32/s1>, Supplemental Figure S1: Isotherm and pore size distribution (inset) of Ni-Ce-ZrO₂ catalysts, Supplemental Table S1: XPS core level electron binding energy of Ni-Ce-ZrO₈ catalysts for different Ni content, Supplemental Figure S2: The stability of Ni6.0 catalyst at 300 °C for 48 h, Supplemental Figure S3: TEM images of (a) fresh and (b) spent Ni6.0 catalysts. Reaction conditions: GHSV = 10,000 h⁻¹, H₂/CO₂ = 4, reaction temperature = 300 °C and reaction time 30 min.

Author Contributions: Conceptualization, V.M., and C.L.; Methodology, V.M., C.L., and T.R.; Validation, V.M., C.L., and T.R.; Formal Analysis, V.M., N.P. (Noppadol Panchan) and N.P. (Nat Phongprueksathat); Investigation, V.M., N.P. (Nat Phongprueksathat), N.P. (Noppadol Panchan), X.G. and A.T.; Resources, V.M. and C.L.; Data Curation, V.M., N.P. (Noppadol Panchan) and T.R.; Writing—Original Draft Preparation, V.M.; Writing—Review and Editing, V.M. and T.R.; Supervision, V.M. Project Administration, V.M. and C.L.; Funding Acquisition, V.M. and C.L. All authors have read and agreed to the published version of the manuscript.

Funding: This research was funded by the National Research Council of Thailand (NRCT) Thai-Chinese joint project (2559-152) and NSFC-NRCT (51661145012).

Acknowledgments: V. Meeyoo would like to thank Chinese Academy of Sciences for his visiting fellowship.

Conflicts of Interest: The authors declare no conflict of interest.

References

1. Tada, S.; Kikuchi, R. Mechanistic study and catalyst development for selective carbon monoxide methanation. *Catal. Sci. Technol.* **2015**, *5*, 3061–3070. [[CrossRef](#)]
2. Karelavic, A.; Ruiz, P. CO₂ hydrogenation at low temperature over Rh/γ-Al₂O₃ catalysts: Effect of the metal particle size on catalytic performances and reaction mechanism. *Appl. Catal. B Environ.* **2012**, *113*, 237–249. [[CrossRef](#)]
3. Pan, Q.; Peng, J.; Sun, T.; Wang, S.; Wang, S. Insight into the reaction route of CO₂ methanation: Promotion effect of medium basic sites. *Catal. Commun.* **2014**, *45*, 74–78. [[CrossRef](#)]
4. De Leitenburg, C.; Trovarelli, A.; Kašpar, J. A Temperature-programmed and transient kinetic study of CO₂ activation and methanation over CeO₂ supported noble metals. *J. Catal.* **1997**, *166*, 98–107. [[CrossRef](#)]
5. Kopyscinski, J.; Schildhauer, T.J.; Biollaz, S.M. Production of synthetic natural gas (SNG) from coal and dry biomass—A technology review from 1950 to 2009. *Fuel* **2010**, *89*, 1763–1783. [[CrossRef](#)]

6. Schild, C.; Wokaun, A.; Koepfel, R.A.; Baiker, A. Carbon dioxide hydrogenation over nickel/zirconia catalysts from amorphous precursors: On the mechanism of methane formation. *J. Phys. Chem.* **1991**, *95*, 6341–6346. [[CrossRef](#)]
7. Upham, D.C.; Derk, A.R.; Sharma, S.; McFarland, E.W.; Metiu, H. CO₂ methanation by Ru-doped ceria: The role of the oxidation state of the surface. *Catal. Sci. Technol.* **2015**, *5*, 1783–1791. [[CrossRef](#)]
8. Xu, J.; Su, X.; Duan, H.; Hou, B.; Lin, Q.; Liu, X.; Pan, X.; Pei, G.; Geng, H.; Huang, Y.; et al. Influence of pretreatment temperature on catalytic performance of rutile TiO₂-supported ruthenium catalyst in CO₂ methanation. *J. Catal.* **2016**, *333*, 227–237. [[CrossRef](#)]
9. Darensbourg, D.J.; Ovalles, C. Catalytic carbon dioxide methanation by alumina-supported mono- and polynuclear ruthenium carbonyls. *Inorg. Chem.* **1986**, *25*, 1603–1609. [[CrossRef](#)]
10. Deleitenburg, C.; Trovarelli, A. Metal-support interactions in Rh/CeO₂, Rh/TiO₂, and Rh/Nb₂O₅ catalysts as inferred from CO₂ methanation activity. *J. Catal.* **1995**, *156*, 171–174. [[CrossRef](#)]
11. Trovarelli, A.; Deleitenburg, C.; Dolcetti, G.; Lorca, J. CO₂ methanation under transient and steady-state conditions over Rh/CeO₂ and CeO₂-promoted Rh/SiO₂: The role of surface and bulk ceria. *J. Catal.* **1995**, *151*, 111–124. [[CrossRef](#)]
12. Park, J.-N.; McFarland, E.W. A highly dispersed Pd–Mg/SiO₂ catalyst active for methanation of CO₂. *J. Catal.* **2009**, *266*, 92–97. [[CrossRef](#)]
13. Schild, C.; Wokaun, A.; Baiker, A. Surface species in CO₂ methanation over amorphous palladium/zirconia catalysts. *J. Mol. Catal.* **1991**, *69*, 347–357. [[CrossRef](#)]
14. Ocampo, M.; Louis, B.; Roger, A.C. Methanation of carbon dioxide over nickel-based Ce_{0.72}Zr_{0.28}O₂ mixed oxide catalysts prepared by sol-gel method. *Appl. Catal. A* **2009**, *369*, 90–96. [[CrossRef](#)]
15. Song, H.; Yang, J.; Zhao, J.; Chou, L. Methanation of carbon dioxide over a highly dispersed Ni/La₂O₃ catalyst. *Chin. J. Catal.* **2010**, *31*, 21–23. [[CrossRef](#)]
16. Tada, S.; Shimizu, T.; Kameyama, H.; Haneda, T.; Kikuchi, R. Ni/CeO₂ catalysts with high CO₂ methanation activity and high CH₄ selectivity at low temperatures. *Int. J. Hydrog. Energy* **2012**, *37*, 5527–5531. [[CrossRef](#)]
17. Tada, S.; Ikeda, S.; Shimoda, N.; Honma, T.; Takahashi, M.; Nariyuki, A.; Satokawa, S. Sponge Ni catalyst with high activity in CO₂ methanation. *Int. J. Hydrog. Energy* **2017**, *42*, 30126–30134. [[CrossRef](#)]
18. Ashok, J.; Ang, M.; Kawi, S. Enhanced activity of CO₂ methanation over Ni/CeCO₂-ZrO₂ catalysts: Influence of preparation methods. *Catal. Today* **2017**, *281*, 304–311. [[CrossRef](#)]
19. Mebrahtu, C.; Abate, S.; Perathoner, S.; Chen, S.; Centi, G. CO₂ methanation over Ni catalysts based on ternary and quaternary mixed oxide: A comparison and analysis of the structure-activity relationships. *Catal. Today* **2018**, *304*, 181–189. [[CrossRef](#)]
20. Ratchahat, S.; Sudoh, M.; Suzuki, Y.; Kawasaki, W.; Watanabe, R.; Fukuhara, C. Development of a powerful CO₂ methanation process using a structured Ni/CeO₂ catalyst. *J. CO₂ Util.* **2018**, *24*, 210–219. [[CrossRef](#)]
21. Agnelli, M.; Kolb, M.; Mirodatos, C. CO hydrogenation on a nickel catalyst: I. kinetics and modeling of a low-temperature sintering process. *J. Catal.* **1994**, *148*, 9–21. [[CrossRef](#)]
22. Agnelli, M.; Swaan, H.; Marquez-Alvarez, C.; Martin, G.; Mirodatos, C. CO hydrogenation on a nickel catalyst. *J. Catal.* **1998**, *175*, 117–128. [[CrossRef](#)]
23. Vance, C.K.; Bartholomew, C.H. Hydrogenation of carbon dioxide on group viii metals: III. effects of support on activity/selectivity and adsorption properties of nickel. *Appl. Catal.* **1983**, *7*, 169–177. [[CrossRef](#)]
24. Kang, S.H.; Ryu, J.H.; Kim, J.H.; Seo, S.-J.; Yoo, Y.D.; Prasad, P.S.S.; Lim, H.J.; Byun, C.D. Co-methanation of CO and CO₂ on the Ni_x-Fe_{1-x}/Al₂O₃ catalysts: Effect of Fe contents. *Korean J. Chem. Eng.* **2011**, *28*, 2282–2286. [[CrossRef](#)]
25. Ocampo, F.; Louis, B.; Kiwi-Minsker, L.; Roger, A.C. Effect of Ce/Zr composition and noble metal promotion on nickel based Ce_xZr_{1-x}O₂ catalysts for carbon dioxide methanation. *Appl. Catal. A Gen.* **2011**, *392*, 36–44. [[CrossRef](#)]
26. Razzaq, R.; Zhu, H.; Jiang, L.; Muhammad, U.; Li, C.; Zhang, S. Catalytic methanation of CO and CO₂ in coke oven gas over Ni–Co/ZrO₂–CeO₂. *Ind. Eng. Chem. Res.* **2013**, *52*, 2247–2256. [[CrossRef](#)]
27. Graça, I.; Gonzalez, L.; Bacariza, C.; Fernandes, A.; Henriques, C.; Lopes, J.; Ribeiro, M.F. CO₂ hydrogenation into CH₄ on NiHNaUSY zeolites. *Appl. Catal. B Environ.* **2014**, *147*, 101–110. [[CrossRef](#)]
28. Rahmani, S.; Rezaei, M.; Meshkani, F. Preparation of highly active nickel catalysts supported on mesoporous nanocrystalline γ-Al₂O₃ for CO₂ methanation. *J. Ind. Eng. Chem.* **2014**, *20*, 1346–1352. [[CrossRef](#)]

29. Aziz, M.; Jalil, A.A.; Triwahyono, S.; Saad, M. CO₂ methanation over Ni-promoted mesostructured silica nanoparticles: Influence of Ni loading and water vapor on activity and response surface methodology studies. *Chem. Eng. J.* **2015**, *260*, 757–764. [[CrossRef](#)]
30. Li, C.; Liu, J.; Wang, F.; He, S.; Chen, H.; Zhao, Y.; Wei, M.; Evans, D.G.; Duan, X. Enhanced low-temperature activity of CO₂ methanation over highly-dispersed Ni/TiO₂ catalyst. *Catal. Sci. Technol.* **2013**, *3*, 2627. [[CrossRef](#)]
31. Lakshmanan, P.; Kim, M.S.; Park, E.D. A highly loaded Ni@SiO₂ core-shell catalyst for CO methanation. *Appl. Catal. A Gen.* **2016**, *513*, 98–105. [[CrossRef](#)]
32. Sun, F.M.; Yan, C.F.; Wang, Z.D.; Guo, C.Q.; Huang, S.L. Ni/Ce–Zr–O catalyst for high CO₂ conversion during reverse water gas shift reaction (RWGS). *Int. J. Hydrog. Energy* **2015**, *40*, 15985–15993. [[CrossRef](#)]
33. Thammachart, M.; Meeyoo, V.; Risksomboon, T.; Osuwan, S. Catalytic activity of CeO₂–ZrO₂ mixed oxide catalysts prepared via sol–gel technique: CO oxidation. *Catal. Today* **2001**, *68*, 53–61. [[CrossRef](#)]
34. Zhou, G.; Liu, H.; Cui, K.; Jia, A.; Hu, G.; Jiao, Z.; Liu, Y.; Zhang, X. Role of surface Ni and Ce species of Ni/CeO₂ catalyst in CO₂ methanation. *Appl. Surf. Sci.* **2016**, *383*, 248–252. [[CrossRef](#)]
35. Westermann, A.; Azambre, B.; Bacariza, M.; Graça, I.; Ribeiro, M.F.; Lopes, J.; Henriques, C. Insight into CO₂ methanation mechanism over NiUSY zeolites: An operando IR study. *Appl. Catal. B Environ.* **2015**, *174*, 120–125. [[CrossRef](#)]
36. Nie, W.; Zou, X.; Chen, C.; Wang, X.; Ding, W.; Lu, X. Methanation of carbon dioxide over Ni–Ce–Zr oxides prepared by one-pot hydrolysis of metal nitrides with ammonium carbonate. *Catalysts* **2017**, *7*, 104. [[CrossRef](#)]
37. Atzori, L.; Rombi, E.; Meloni, D.; Sini, M.F.; Monaci, R.; Cutrufello, M.G. CO and CO₂ Co-Methanation on Ni/CeO₂–ZrO₂ soft-templated catalysts. *Catalysts* **2019**, *9*, 415. [[CrossRef](#)]
38. Vrijburg, W.L.; Helden, J.W.A.; Parastaev, A.; Groeneveld, E.; Pidko, E.A.; Hensen, E.J.M. Ceria-zirconia encapsulated Ni nanoparticles for CO₂ methanation. *Catal. Sci. Technol.* **2019**, *9*, 5001–5010. [[CrossRef](#)]



© 2019 by the authors. Licensee MDPI, Basel, Switzerland. This article is an open access article distributed under the terms and conditions of the Creative Commons Attribution (CC BY) license (<http://creativecommons.org/licenses/by/4.0/>).